

# THE CAUSES OF FOEHN WARMING IN THE LEE OF MOUNTAINS

BY ANDREW D. ELVIDGE AND IAN A. RENFREW

A first quantitative investigation into the causes of foehn warming in the lee of mountain ranges demonstrates the importance of three physical mechanisms, including one previously neglected.

**S**ocietal and environmental impacts of the warming experienced in the lee of mountains, known as the foehn warming effect, are significant and diverse. This warming can be spectacular (e.g., 25°C in an hour; Richner and Hächler 2013) and is typically accompanied by a decrease in humidity and accelerated downslope winds. The notoriety of these foehn winds has led to recognition by various local terms: among others, the Chinook and Santa Ana of North America and the Zonda of Argentina. The warmth brought by the foehn has implications for agriculture, ecosystems, and climate systems. It can increase the risk of avalanches or floods (Barry 2008), melt glaciers, and contribute to ►

Rotor cloud revealing overturning and turbulence above the lee slopes of the Antarctic Peninsula during a foehn event (Case A in this study). Photo by A. Elvidge.

the disintegration of ice shelves (Cook et al. 2005; Kuipers Munneke et al. 2012). Foehn windstorms regularly cause damage to property and infrastructure (Whiteman and Whiteman 1974; Richner and Hächler 2013), and the combination of warm, dry air and high wind speeds promotes the ignition and rapid spread of wildfires (Westerling et al. 2004; Gedalof et al. 2005; Sharples et al. 2010). In California, Santa Ana winds are responsible for the majority of major wildfires, including 12 fires in October 2003 that burnt an area of over 300,000 ha, causing more than \$1 billion (U.S. dollars) in property damage (Westerling et al. 2004; Ahrens 2012). Accurate forecasting of foehn events is a challenge for hazard assessment and management, one that is made significantly harder by a lack of quantitative understanding of the causes of foehn warming.

**PARADIGMS OF THE FOEHN.** Traditionally foehn winds are defined as any “warm, dry wind descending in the lee of a mountain range” (Brinkmann 1971, p. 230; Ahrens 2012; Barry 2008). However, this definition begs two critical questions: 1) what is the foehn warm and dry relative to and 2) why is the foehn warm and dry? While such imprecision is perhaps appropriate in describing something that is an everyday occurrence for many, it also reflects the difficulty in concisely defining a phenomenon that is not fully understood. Indeed Brinkmann (1971, p. 238) challenges his own definition (above) by concluding, “Since the search for the definition of a phenomenon is, by necessity, the search for its cause, and since the true causes are still poorly understood, the question remains: what is foehn?” Recent advances have provided the tools to better understand foehn flows, and they support a Lagrangian definition as the framework for investigation (cf. WMO 1992); for example, the

foehn is a downslope wind in the lee of a mountain that is accelerated, warmed, and dried as a result of the orographic disturbance on the prevailing flow.

The first scientific accounts put forward two mechanisms for foehn warming and drying, for example, Hann (1901); also see Beran (1967), Barry (2008), and Richner and Hächler (2013). The first is the sourcing of foehn air from higher, potentially warmer and dryer altitudes upwind of the mountain barrier due to the blocking of low-level flow by the mountain. This mechanism is here termed *isentropic drawdown* and is illustrated in Fig. 1a. Note that *isentropic drawdown* is likely to be associated with the drawdown of drier air too, though there may be occasions when leeside drying does not accompany leeside warming (e.g., Gaffin 2002). Flow blocking is characteristic of a non-linear flow regime, where the speed of the approaching stably stratified flow is insufficient for ascent from low levels over the mountain (Smith 1990). The second is the more well-known “thermodynamical” foehn theory, whereby cooling during uplift on the windward slopes promotes condensation, cloud formation, and subsequently precipitation leading to moisture removal and irreversible latent heating (the *latent heating and precipitation* mechanism; Fig. 1b). Considerable orographic uplift and cloud formation are characteristic of a linear flow regime, where the approaching flow is strong enough to overcome buoyancy forces and ascend from low levels over the mountain (Smith 1990). These two mechanisms have been widely discussed in the literature (e.g., Scorer 1978; Seibert 1990; Richner and Hächler 2013). However, two other foehn mechanisms also exist: turbulent sensible heating and drying of the low-level flow via *mechanical mixing* (Fig. 1c) above rough, mountainous terrain in a stably stratified atmosphere (Scorer 1978; Ólafsson 2005) have always been dismissed as unimportant or, more commonly, simply neglected, and *radiative heating* (Fig. 1d) of the low-level lee side due to the dry, cloud-free foehn conditions (Hoinka 1985; Ólafsson 2005) tends not to have been explicitly considered as a foehn mechanism.

Interestingly, for several decades *isentropic drawdown* was all but lost as an explanation for the foehn effect as the more textbook-friendly *latent heating and precipitation* mechanism was preferred, becoming a classic example of thermodynamics changing the weather (Seibert 1990; Richner and Hächler 2013). In fact, in popular media and nonacademic scientific articles, this bias is still common. This is despite some recent case studies qualitatively indicating that latent heating is of secondary importance (Seibert 1990; Ólafsson 2005), in contrast to others that indicate the opposite (Seibert

**AFFILIATIONS:** ELVIDGE AND RENFREW—School of Environmental Sciences, University of East Anglia, Norwich, United Kingdom

**CORRESPONDING AUTHOR:** Dr. A. D. Elvidge, Atmospheric Processes and Parameterizations, Met Office, FitzRoy Road, Exeter, Devon, EX1 3PB, United Kingdom  
E-mail: andy.elvidge@metoffice.gov.uk

The abstract for this article can be found in this issue, following the table of contents.

DOI:10.1175/BAMS-D-14-00194.1

In final form 24 April 2015  
©2016 American Meteorological Society



This article is licensed under a [Creative Commons Attribution 4.0 license](https://creativecommons.org/licenses/by/4.0/).

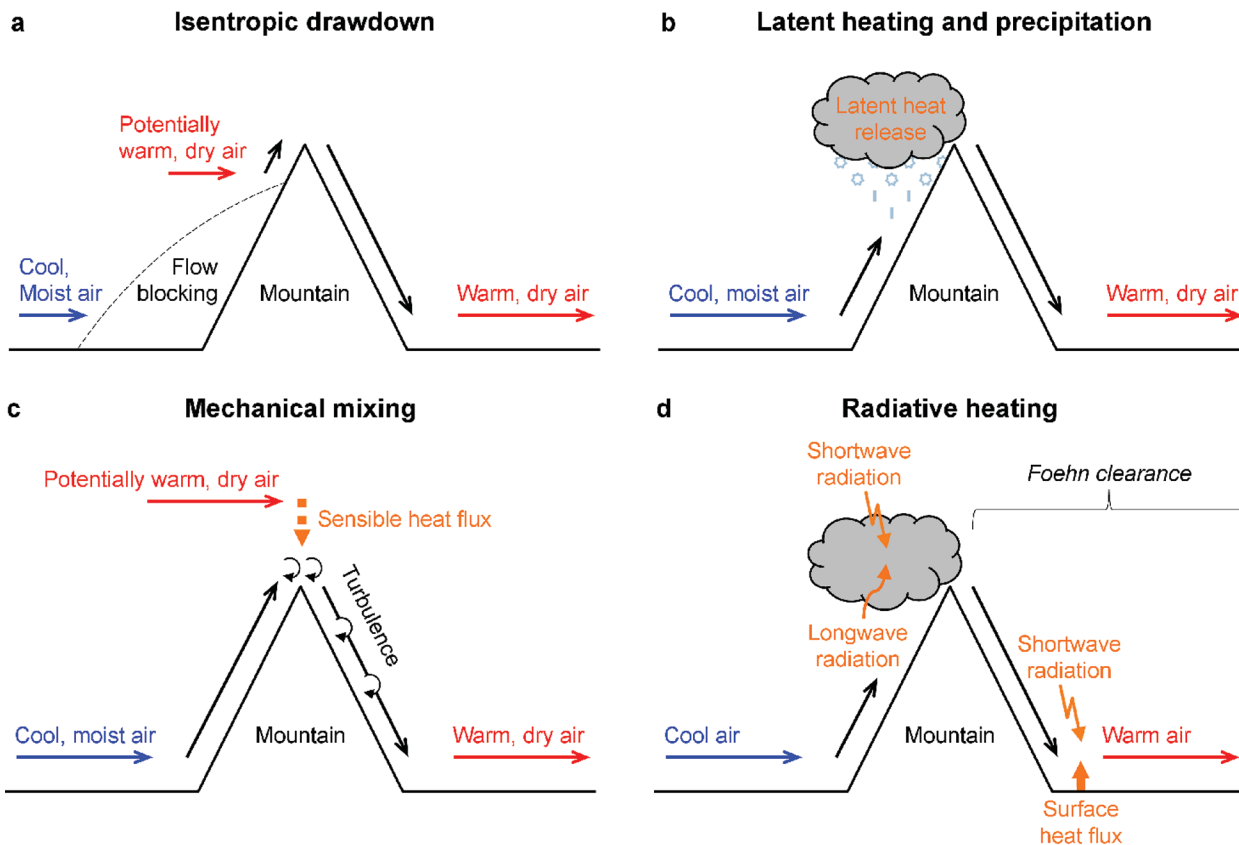


**FIG. 1.** Foehn warming mechanisms. (a) Upwind of the mountain, cool, moist air can be blocked allowing potentially warmer, drier air to be advected isentropically down the lee slopes. (b) Without flow blocking, there is ascent on the windward slopes so the air cools, leading to condensation and latent heat release that reduces the cooling; precipitation removes the condensed water so that descent on the lee side is dry, which increases the (pressure related) warming leading to higher leeside temperatures. (c) As cool, moist air passes over the mountain, it will mix mechanically with the overlying air mass; for a statically stable atmosphere, this is potentially warmer (and usually drier) and so corresponds to a turbulent flux of sensible heat into the foehn flow (and a turbulent flux of moisture out of it). (d) Associated with the mechanisms described in (a)–(c), there is often clear, dry air on the downwind slopes, the “foehn clearance,” and cloud on the upwind slopes; this situation encourages radiative flux convergence and thus warmer air on the lee side.

et al. 2000; Richner and Hächler 2013). Here, for the first time, we are able to quantitatively address the question “what causes foehn warming?” We employ a novel Lagrangian heat budget model that uses trajectories from high-resolution numerical model output to focus on three representative case studies.

**AN IDEAL NATURAL LABORATORY.** The Antarctic Peninsula provides one of the best natural laboratories in the world for the study of foehn: it presents a consistently high (up to ~2300 m), broad (~100 km), and long (~1500 km) quasi-2D barrier to the prevailing westerly flow, with homogeneous and relatively smooth upwind (maritime) and downwind (ice shelf) surface boundaries (see Fig. 2). The three foehn events examined have westerly flow across the peninsula onto the Larsen C Ice Shelf (LCIS) and

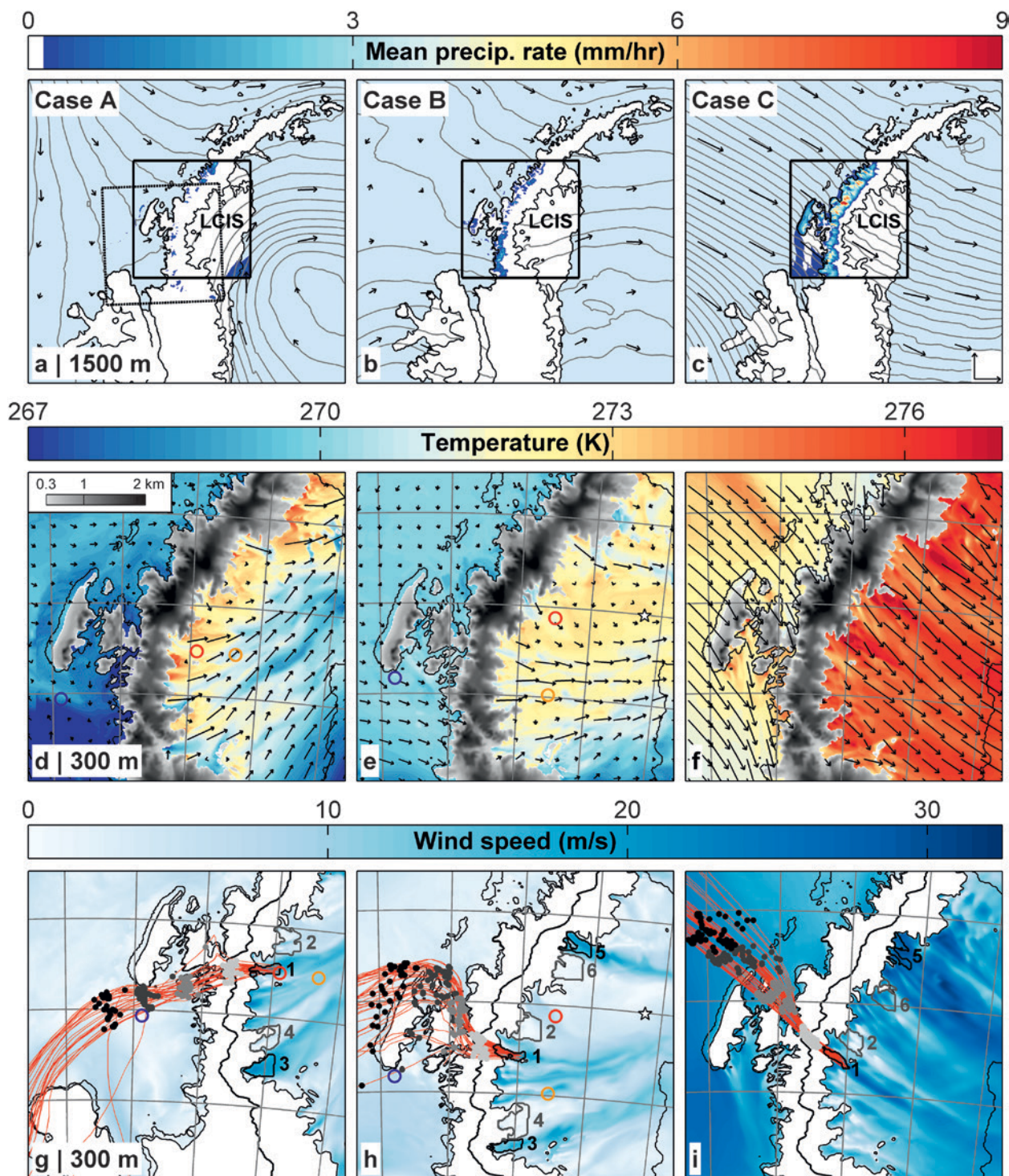
occurred during the austral summer of 2010/11. Two of them (cases A and B) are documented by aircraft observations (Elvidge et al. 2015, 2016), and all three have been simulated using the Met Office Unified Model (see sidebar on “Observations and simulations of three westerly events”).

Upwind (west) of the peninsula, cases A and B were characterized by relatively weak upwind flow, while in case C a large-scale pressure gradient drove strong northwesterly flow across the barrier (Figs. 2a–c). The weak winds of case A combined with a statically stable atmosphere and an elevated inversion (~1,250 m) to produce a strongly nonlinear flow regime (Elvidge et al. 2016), in which considerable flow blocking is associated with little orographic precipitation (Fig. 2a). Conversely, the strong winds and weaker static stability of case C lead to a relatively linear flow

regime with considerable orographic uplift and high precipitation rates (peaking at  $\sim 12$  mm h $^{-1}$ ; Fig. 2c). Case B resides somewhere between the two in terms of flow regime linearity and precipitation (Fig. 2b).

At low levels above the LCIS, southwesterly to northwesterly foehn winds are apparent in all three cases (Figs. 2d–f). In contrast to climatology, conditions to the east of the peninsula are warmer

than those to the west, implying foehn warming. For case A, the warming (up to 5 K) and also drying are apparent in observations taken from aircraft profiles (Fig. 3). Here, the upwind profile used for temperature was flown 4–5 h prior to the two downwind profiles (see sidebar on “Observations and simulations of three westerly events”), roughly reflecting the time taken for air to cross the barrier. Note that



in both the observations and the model simulation leeside temperatures decrease with distance downwind of the mountains (Figs. 2d, 3a). For case B, aircraft observations again show warmer conditions on the lee side of the mountain range, indicating a foehn event. Unfortunately the profiles here are not Lagrangian; the upwind profile was flown 1–2 h after the downwind profiles.

The evolution of foehn conditions at the eastern reaches of the LCIS during case B is illustrated by a time series of atmospheric soundings in Fig. 4. On the evening of 26 February 2011, conditions are stagnant and cool over the ice shelf. Over the course of 27 February, westerly winds throughout the depth of

the lower atmosphere bring about a warming (3–4 K between 200 and 500 m) and drying, as illustrated by the downward-sloping potential temperature and specific humidity contours with time. Note that below ~200 m, a surface-forced diurnal variation is superposed on the foehn signature.

The numerical model generally performs well in its simulation of cases A and B. In Fig. 3, the model reproduces both upwind and downwind profiles of temperature and humidity to a high degree of accuracy (typically within 0.5 K and 0.2 g kg<sup>-1</sup>), especially at low levels. This implies the model is able to accurately capture the warming of air parcels as they cross the peninsula. Further downwind of the

## OBSERVATIONS AND SIMULATIONS OF THREE FOEHN EVENTS

Aircraft measurements were made by an instrumented De Havilland Canada Twin Otter aircraft [for details see Fiedler et al. (2010)]. Observations from two flights on 5 February 2011 (case A) and one flight on 27 January 2011 (case B) are shown in Fig 3. For Case A, aircraft data comprise upwind profiles at 1130 and 1330 UTC over Marguerite Bay (blue circle in Figs. 2d,g marks the locations) and downwind profiles at 1530 and 1600 UTC over LCIS and Whirlwind Inlet (orange and red circles in Figs. 2d,g). Note that the first upwind profile for humidity is not available owing to an instrument malfunction, so the second upwind profile is shown in Fig. 3. Case B aircraft data comprise an upwind profile at 1800 UTC over Marguerite Bay (blue circle in Figs. 2e,h) and downward profiles at 1600 and 1630 UTC over the LCIS (red and orange circles in Figs. 2e,h). Further aircraft observations are

shown in Elvidge et al. (2015, 2016). During case B, Vaisala radiosondes were launched from a camp toward the eastern reaches of the LCIS (star in Figs. 2e,h) at 1800 UTC on 26 January, and then 6 hourly between 1200 UTC on 27 January and 0600 UTC on 28 January 2011.

The Met Office Unified Model (the MetUM), version 7.6, MetUM, version 7.6, which is used for operational numerical weather prediction and climate prediction (Davies et al. 2005), has been used [configured following Elvidge et al. (2015)]. Our highest-resolution domain has a grid spacing of 1.5 km and 70 vertical levels. Such high resolution was necessary to adequately resolve the complex flow fields and large vertical velocities generated by the Antarctic Peninsula's steep and complex orography. This model and configuration has previously demonstrated considerable skill in reproducing the key features of westerly

foehn flow over the peninsula (Elvidge et al. 2015, 2016) and other strong wind events near steep orography (Orr et al. 2014). The MetUM 1.5-km simulations were initiated at 0600 UTC 4 February 2011 for case A, 1800 UTC 26 January 2011 for case B, and 0600 UTC 15 November 2010 for case C. Each was nested within a larger regional domain with 4-km grid spacing initiated 6 h earlier, which in turn was nested within a global domain with 25-km grid spacing. The majority of analysis presented is from the MetUM 1.5-km simulations. In addition to the standard 1.5-km domain, a southwest-shifted domain was used in case A, where necessary, to avoid the premature departure of back trajectories (see Fig. 2). Note each of these case A simulations was nested within the same 4-km simulation and reproduced the same major flow features (where there was an overlap), that is, comparable foehn warming, jets, and wakes.

**FIG. 2. Three foehn events over the Antarctic Peninsula simulated by a high-resolution numerical weather prediction model. All plots show conditions in cases (left) A, (middle) B, and (right) C at the time of back trajectory initiation. (a)–(c) Pressure (contours every 1 hPa) and wind vectors at 1500 m MSL for the 4-km-resolution model domain; insets are mean precipitation rates for the 1.5-km resolution model domains. LCIS is marked. The scaling vectors in (c) illustrate 20 m s<sup>-1</sup> [for panels (a)–(f)]. (d)–(f) Temperature (shading) and wind vectors at 300 m MSL for the 1.5-km-resolution domain. Model topography is shaded in gray. (g)–(i) Wind speed at 300 m MSL and also the peninsula's topographic crest as a bold line for the 1.5-km-resolution domain [the southwest-shifted domain in (g)]. On the lee side, six regions are outlined, three of which (in black) correspond to inlets that experience foehn jets; the other three (in gray) correspond to wake areas to the north (N of) or south (S of) each inlet. The regions are labeled as follows: 1) Whirlwind Inlet, 2) N of Whirlwind Inlet, 3) Mobil Oil Inlet, 4) N of Mobil Oil Inlet, 5) Cabinet Inlet, and 6) S of Cabinet Inlet. Back trajectories (red lines) are plotted from WI, with the grayscale dots marking points 0, 50, 100, and 150 km upwind of the peninsula's crest along the back trajectories. Note only every fourth back trajectory is shown. Colored circles and stars are locations for Figs. 3 and 4.**

peninsula, in situ changes in winds, temperature, and humidity during case B are also generally well simulated (Fig. 4). The model captures the transition between cool, moist, and stagnant conditions to warmer, drier foehn conditions with stronger, westerly winds, followed by the weakening of winds and stabilizing of temperatures and humidities on the morning of 28 February 2011. There are some shortcomings: for example, the model overestimates low-level humidities prior to the foehn event and exaggerates static stability and vertical humidity gradients throughout case B. More evidence of this model's generally high level of skill in reproducing these foehn events can be found in two recent publications: Elvidge et al. (2015) provide validation of

upwind conditions, the broad-scale foehn warming, and the structure and magnitude of foehn winds for cases A and B. Elvidge et al. (2016) provide validation of orographic gravity waves and turbulence over the mountains for case A.

In all three cases, the leeside low-level wind field is distinguished by a series of jets emanating from the mouths of major inlets on the peninsula's east coast, separated by regions of weaker flow, termed here "wakes" (Figs. 2g–i). These "foehn jets" (Elvidge et al. 2015) are characterized by higher wind speeds than upwind, the flow having been accelerated across the mountains. They are the result of gap flows (Mayr et al. 2007) through mountain passes along the peninsula's crest (Elvidge et al. 2015). The jets are generally cooler (Figs. 2d–f) and moister than adjacent wake regions because of a dampening of the foehn effect, a consequence of the lower terrain traversed by the gap flows (Elvidge et al. 2015). Back trajectories for jets emanating from Whirlwind Inlet (WI) (Figs. 2g–i) show a clustering in space that is typical of the jets and wakes and suggest a common upwind source region. It also implies that average back trajectories can be treated as representative of the foehn flow impacting that region. Note that the Lagrangian model used for calculating the back trajectories is described in the sidebar on "Lagrangian modeling." Figure 5 shows the mean back trajectory characteristics for all three cases for Whirlwind Inlet. It reveals various features in the Lagrangian evolution of a foehn air parcel: upwind ascent on approaching the peninsula, leeside descent, a net drawdown of flow and/or diabatic warming, and moisture loss across the barrier. These features are illustrative of each of the jet and wake regions and thus the foehn flow in general.

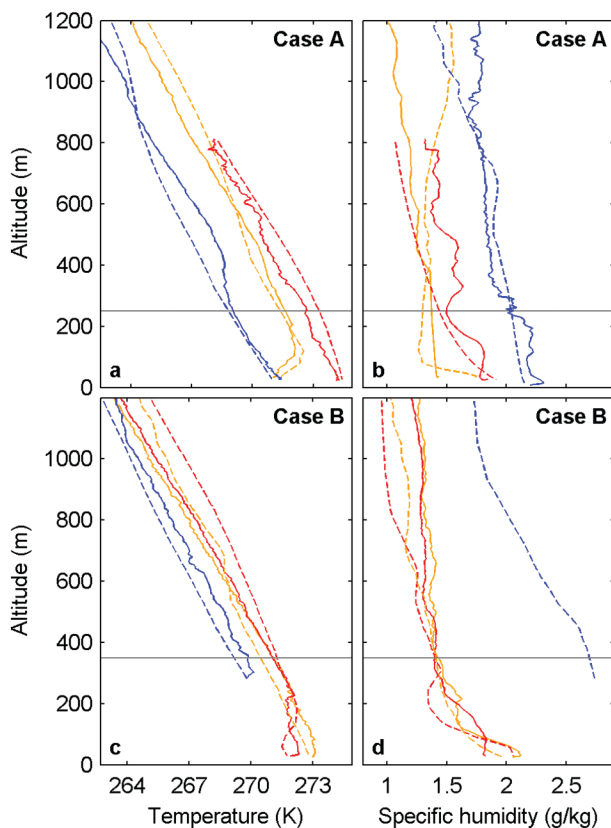


**FIG. 3. Profiles of temperature and specific humidity upwind and downwind of the Antarctic Peninsula. The profiles are from instrumented aircraft observations (solid lines) and corresponding model output (dashed lines) for cases A and B. The upwind profiles (from Marguerite Bay) are plotted in blue, and the downwind profiles are plotted in red and orange. The locations of the profiles are marked in appropriate panels of Fig. 2 as circles of the same color. Note that, owing to an instrument malfunction, the observed upwind humidity profile is not available for case B. The horizontal gray lines mark the altitude of back trajectory initialization.**

**QUANTIFYING FOEHN WARMING.** Figure 6a illustrates the key features of a novel Lagrangian heat budget model devised to quantify and attribute foehn warming contributions to particular foehn mechanisms. The model follows an air parcel from point B (upwind) to point C near the surface in the immediate lee of the peninsula where the foehn flow has the most impact and where the back trajectories are initiated. Point B is in undisturbed flow and so must be further upwind than the Rossby radius of deformation (Hunt et al. 2001), which is  $\sim 150$  km here (Elvidge et al. 2015). Point A is below point B and at the same height as C.

The *foehn warming* is the temperature change induced by the orographic disturbance, defined as  $\Delta^{FT} \approx T_C - T_A$ , where  $T_C$  is the mean trajectory

temperature at C and  $T_A$  is the mean temperature at A (at the time the trajectories pass B). It is the sum of five contributions (Fig. 6a), four of which can be equated directly to the foehn mechanisms of Fig. 1. The *isentropic draw-down* contribution  $\Delta^{ID}T$  is due to the sourcing of air from point B, rather than A, and so is the mean difference in  $\theta$  between trajectories at B and simultaneous conditions at A. The other three mechanisms can be determined from Lagrangian air parcel changes. The *latent heating and precipitation* contribution  $\Delta^{LHT}$  is due to changes in  $\theta - \theta_e$ , with convergence indicating latent heat gain (from condensation or freezing) and divergence indicating latent heat loss (from evaporation or melting). Changes in air parcel  $\theta_e$  reflect the remaining diabatic contributions from *mechanical mixing* leading to sensible heating  $\Delta^{SHT}$  and *radiative heating*  $\Delta^{RHT}$ . These two mechanisms can be isolated by computing  $\Delta^{RHT}$  along the foehn trajectories using numerical model output. Note that  $\Delta^{RHT}$  is not shown as—

together with convective contributions to  $\Delta^{SHT}$  (see sidebar on “Lagrangian modeling”)—it is insignificant in our cases (contributing less than 0.1 K of leeside warming), probably as a result of the large solar zenith angles and the clear, dry air. The final contribution to the temperature budget is associated with any foehn-induced cross mountain pressure gradient  $\Delta^{APT}$ . During a foehn event, a leeside low pressure anomaly is generated as a result of foehn warming and flow blocking (Gaffin 2009), which leads to a minor leeside cooling contribution.

Foehn temperature anomalies and warming contributions by each mechanism are shown in Figs. 6b–d for the three cases and six regions. Case A

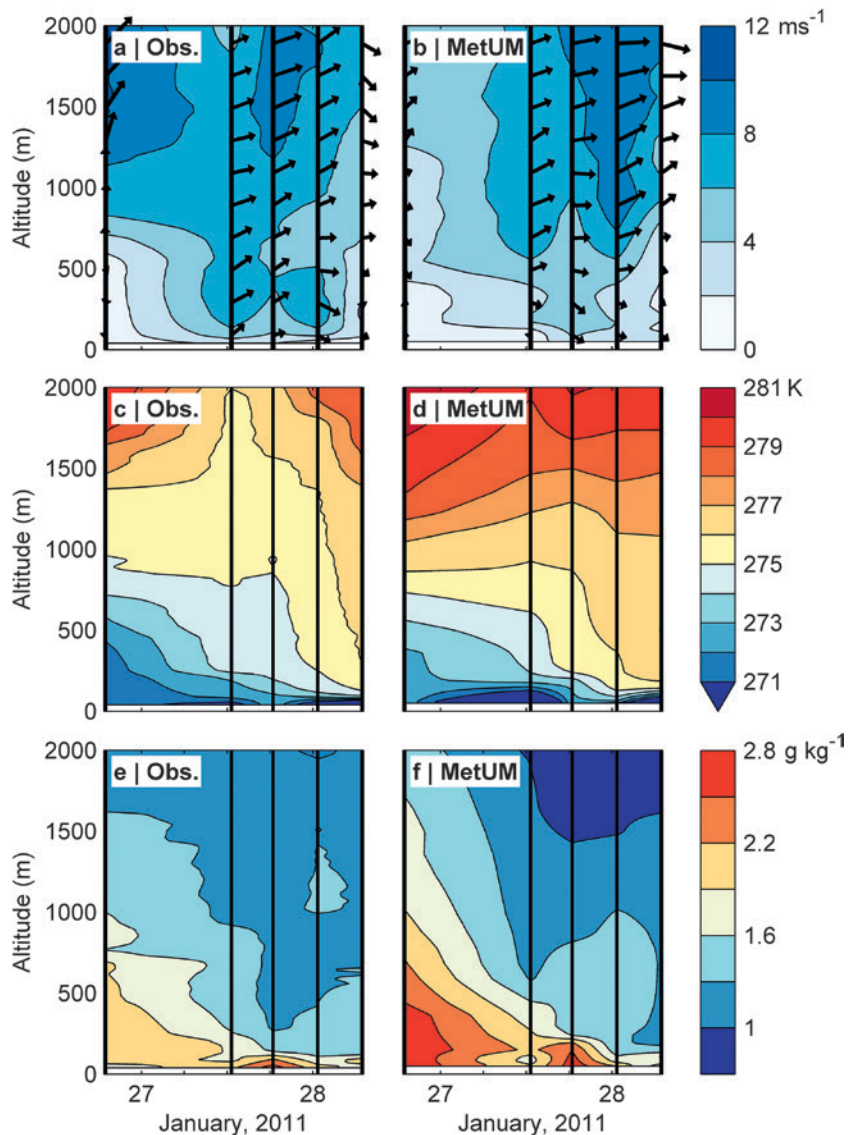


**FIG. 4.** Incursion and evolution of foehn conditions above the LCIS during case B. Time series of (a),(b) wind velocity, (c),(d) potential temperature, and (e),(f) specific humidity interpolated from five soundings (vertical black lines) from radiosondes released from near the eastern edge of the LCIS (star in Figs. 2e,h) and from corresponding model profiles. Vectors in (a) and (b) indicate wind speed and horizontal wind direction (e.g., a rightward-pointing arrow denotes a westerly wind).

generally exhibits the greatest leeside warming, with  $\Delta^FT$  between 1.7 and 5.1 K, compared to 1.1–3.6 K in case B and 1–3.7 K in case C. The trajectory-derived temperature changes are consistent with the observed and simulated low-level near-Lagrangian warming shown in Fig. 3 (case A) and in situ warming shown in Fig. 4 (case B), albeit for a location farther east on the ice shelf. Note the foehn warming is generally greater in the wake regions than the adjacent jet regions.

In case A, *isentropic drawdown* is the dominant mechanism, consistent with having the highest

source altitude for foehn air out of the three cases (evident for WI in Figs. 5a,d,g and for all regions in Figs. 6b–d). These contributions are the largest of any of the mechanisms, peaking at 8 K south of the Cabinet Inlet (CI) wake. In case C, *latent heating and precipitation* is the dominant mechanism, consistent with having the highest upwind humidities (Figs. 5c,f,i) and greatest orographic uplift (Figs.

5a,d,g) and, as a result, the greatest precipitation rates (Figs. 2a–c) and moisture losses of the three cases. In case B, there is no single dominant mechanism. Sensible heating due to *mechanical mixing* provides the largest contribution in two of the five regions, peaking at ~2 K north of WI. This reflects greater orographic uplift (of potentially cool air over rough orography) than in case A together with less precipitation due to drier air than in case C (Figs. 5f,i). Note in case B, WI trajectories undergo sensible heating throughout their approach to the Antarctic Peninsula, perhaps owing to turbulent mixing over the rough terrain of Adelaide Island (Fig. 2h). In general, the jet regions have similar, but smaller, foehn heating contributions to the adjacent wake regions; that is, they experience a dampened foehn effect.

Taking an overview of the 15 heat budgets shown, it is clear that all three foehn warming mechanisms are important. The two established mechanisms of *isentropic drawdown* and *latent heating and precipitation* contribute the largest single warming contributions of 8 K during case A and 4 K during case C and are each the dominant mechanism in 6 out of 15 cases. *Mechanical mixing* is also important, providing over 20% of the total warming in 7 out of 15 cases and being the dominant mechanism in 3 cases. In only 5 out of 15 cases is its magnitude less than 20% of the total warming. Clearly, none of the three mechanisms can be neglected, and therefore each must be well represented for accurate simulation and prediction of foehn events. This suggests that a detailed analysis of the representation of each mechanism has the potential to pinpoint the problems that can still exist in numerical weather prediction forecasts of foehn flows (Richner and Hächler 2013).

It should be noted that *mechanical mixing* contributions will be dependent on the subgrid-scale turbulence scheme employed (Zängl et al. 2004). The model we are using [the Met Office’s Unified Model (MetUM); see sidebar on “Observations and simulations of three westerly events”] employs a nonlocal 1D turbulence scheme (Lock et al. 2000) that has been extensively tested against observations and is highly competitive in terms of its performance (e.g., Svensson et al. 2011; Boutle et al. 2014). This scheme has previously shown considerable skill in complex terrain, enabling realistic representation of temperature variability in valley cold pools, where vertical turbulent heat transport is found to dominate the heat budget (Vosper et al. 2013, Vosper et al. 2014). In this suite of experiments, those that employed the 1D turbulence scheme were found

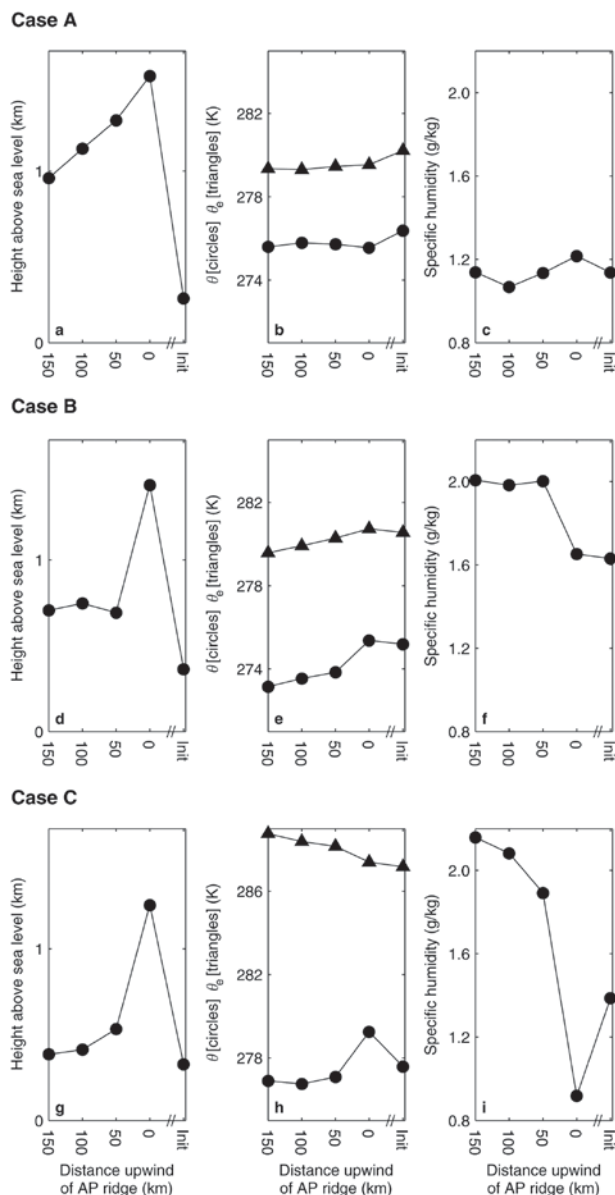
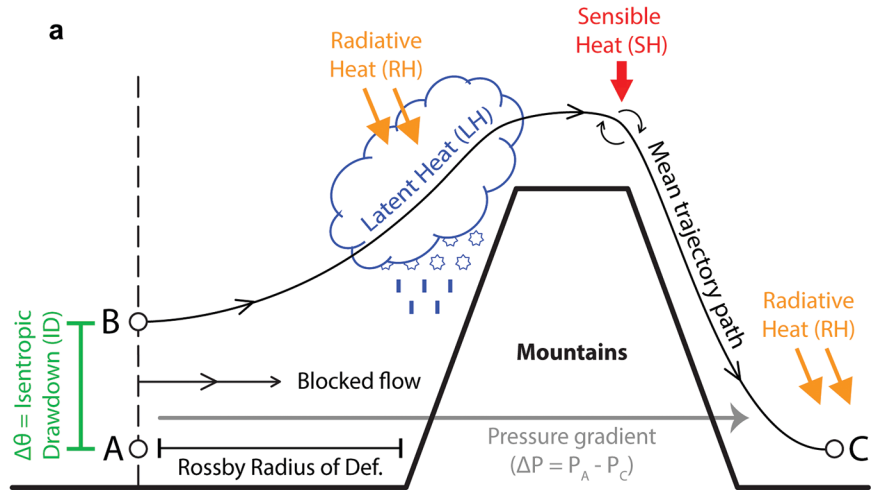


**FIG. 5.** Mean air parcel properties following back trajectories during foehn events. The air parcel properties shown are height above MSL, potential temperature ( $\theta$ , circles), equivalent potential temperature ( $\theta_e$ , triangles), and specific humidity. Mean back trajectory properties are plotted against distance upwind of the peninsula’s crest and initiated in the jet region of Whirlwind Inlet.

to yield near-identical results to those using a 3D Smagorinsky scheme (S. Vosper 2015, personal communication). The proven skill of the turbulence scheme we use, along with the model’s success in simulating temperatures in the immediate lee of the peninsula (see, e.g., Fig. 3)—implying no large or systematic discrepancy in any one term—provides confidence that our new foehn warming paradigm is well founded. We acknowledge, however, that there is some uncertainty with this contribution; for example, modeled turbulent kinetic energy in foehn flows has previously been found to be underestimated (Lothon et al. 2003; Richner and Hächler

2013), implying an underestimate in the *mechanical mixing*–driven sensible heating contribution. In future work, we will examine the sensitivity of the heating contributions to the parameterization of turbulence further. An appropriate representation of turbulence in foehn flows has the potential to improve their prediction and that of related hazards, potentially mitigating adverse societal impacts (e.g., Meyers and Steenburgh 2013).

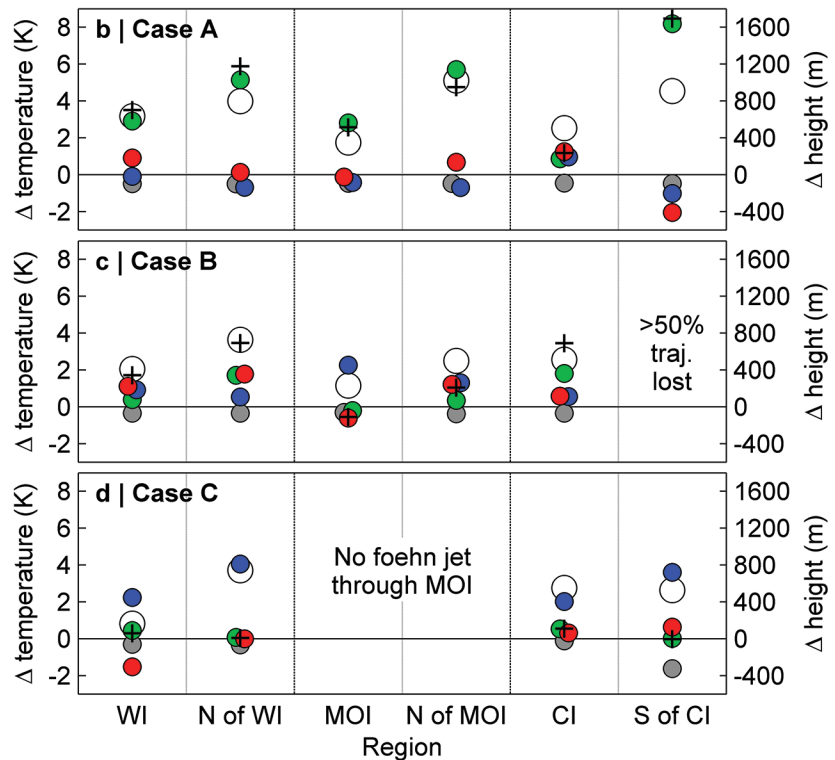
**FIG. 6. Foehn heating contributions.** (a) Lagrangian heat budget model for an air parcel passing over a mountain, from point B to point C, and experiencing the following foehn warming mechanisms: *isentropic drawdown*  $\Delta^{ID}T$  (green), *latent heating and precipitation*  $\Delta^{LHT}$  (blue), *sensible heating due to mechanical mixing*  $\Delta^{SHT}$  (red), *radiative heating*  $\Delta^{RHT}$  (orange), and *pressure gradient-related cooling*  $\Delta^{APT}$  (gray). These contributions sum to a total foehn heating  $\Delta^F T$ ; see text for further details. (b)–(d) The foehn heating contributions as a change in temperature (K). The total foehn warming is plotted as a large open circle (○) and the heating contributions are color coded: *isentropic drawdown* (●), *latent heating and precipitation* (●), *sensible heating through mechanical mixing* (●), and *pressure gradient cooling* (●). The *radiative heating* contribution is negligible. Also shown is the cross-peninsula descent (+). Note that the circles are sometimes offset to improve clarity. The 15 foehn flow heat budgets are illustrated over three case studies and six back trajectory initiation regions (see Figs. 2g–i).



$$\Delta^F T = \Delta^{ID}T + \Delta^{LHT} + \Delta^{SHT} + \Delta^{RHT} + \Delta^{APT}$$

$$T_C - T_A = \theta_B - T_A + (\theta_C - \theta_{e_c}) - (\theta_B - \theta_{e_b}) + \theta_{e_c} - \theta_{e_b} - \int_B^C \Delta^{RH} \theta + \int_B^C \Delta^{RHT} \theta + T_C - \theta_C$$

Reference pressure for  $\theta = P_A$



## LAGRANGIAN MODELING

The trajectory model Lagranto (Wernli and Davies 1997) is employed to provide a Lagrangian analysis of the cross-peninsula flow. MetUM 1.5-km data were used as input for the calculation of back trajectories initiated at every grid point within assigned regions to the east (lee side) of the peninsula at 1000 UTC 5 February 2011 during case A, 0000 UTC 28 January 2011 during case B, and 2200 UTC 15 November 2010 during case C. These times coincide roughly with a peak in the foehn warming; other trajectory analysis, with slightly different trajectory initiation times and from the southwesterly domain, yielded similar results. Lagranto is run backward in time for up to 24 h at a resolution of 3 min; a small time step was necessary because of the high spatial resolution of the simulations. The evolution of physical variables along these Lagrangian paths is then evaluated. The trajectory initiation regions consist of three inlets subject to foehn jets, Whirlwind Inlet

(WI), Mobil Oil Inlet (MOI), and Cabinet Inlet (CI), and three wake regions, to the north of WI (N of WI) and MOI (N of MOI) and to the south of CI (S of CI) (see Fig. 2). For case A, data from the southwest-shifted domain are used as input for trajectories that were initiated within the four southernmost regions. For case B, more than 50% of the S of CI trajectories are lost owing to an unphysical intersection with the orography (Elvidge et al. 2015b; Miltenberger et al. 2013) and so an analysis of these is not possible. For case C, trajectories are not initiated within the MOI and N of MOI regions as there was little cross-peninsula flow here (as apparent in Fig. 2f), and for the CI and S of CI trajectories, distances of 50 and 100 km upwind (respectively) are used for the undisturbed flow (rather than the usual 150 km) owing to the exit of trajectories from the model domain.

The Lagrangian heat budget model used to quantify foehn warming

contributions is outlined in the main text; however, a couple of additional details are noted here. First,  $\theta_e$  along the trajectories is conserved for latent heat exchange owing to condensation and evaporation (Bolton 1980) and also owing to freezing and melting. These latter phase changes are important in our case studies owing to significant cloud ice contents; virtually all precipitation above the peninsula falls as snow rather than rain. Consequently,  $\Delta^{LH}T$  is the net effect on Lagrangian temperature changes owing to all latent heat processes. Second, in addition to orographically driven mechanical mixing with potentially warmer air, contributions toward  $\Delta^{SH}T$  could conceivably be due to sensible heat exchange from the surface, which depends on radiatively driven changes in surface temperature. This surface-derived contribution is negligible in our cases owing to stable stratification but in general should be considered.

**CONCLUSIONS.** A novel heat budget model employed in an ideal natural laboratory has provided the first quantitative evaluation of the causes of foehn warming, demonstrating that either of the established foehn warming mechanisms (*isentropic drawdown* and *latent heating and precipitation*), as well as a previously neglected mechanism (*mechanical mixing* due to turbulence), can be chiefly responsible for leeside warming. This discovery suggests a new paradigm for foehn warming in the lee of mountains is required, one in which all three of these heating mechanisms are important and any can dominate. In addition, a fourth mechanism (*radiative heating*), found to be unimportant here (at most 0.1 K), cannot always be discounted and may be significant in other foehn-prone regions, for example, where radiative fluxes are greater. The importance of each mechanism depends upon the orographically forced flow dynamics and meteorological conditions and so varies from case to case. Previous assertions on the dominance of one mechanism over another must be the result of regional or case study specifics and are not general. Indeed, future work should include the application of our Lagrangian heat budget model to foehn winds elsewhere in the world and also to idealized cases to establish the general applicability of our new paradigm.

**ACKNOWLEDGMENTS.** The authors thank J. C. King, A. Orr, T. Lachlan-Cope, M. Joshi, and G. W. K. Moore for useful discussions and comments. We acknowledge invaluable help with the numerical modelling from M. Weeks, S. Webster, S. Vosper, S. L. Gray, and M. Sprenger. The simulations were carried out on the joint Met Office/NERC MONSooN computing system. We acknowledge the support of the British Antarctic Survey's air unit and field operations team in obtaining the aircraft observations—in particular the leadership of Tom Lachlan-Cope—as well as A. Kirchaessner, P. Kuipers-Munnke, and J. C. King for the radiosonde data. This research was funded by NERC (NE/G014124/1) as part of the Orographic Flows and Climate over the Antarctic Peninsula (OFCAP) project.

## REFERENCES

- Ahrens, C. D., 2012: *Meteorology Today: An Introduction to Weather, Climate, and the Environment*. Cengage Learning, 640 pp.
- Barry, R. G., 2008: *Mountain Weather and Climate*. 3rd ed. Cambridge University Press, 506 pp.
- Beran, D. W., 1967: Large amplitude lee waves and chinook winds. *J. Appl. Meteor.*, **6**, 865–877, doi:10.1175/1520-0450(1967)006<0865:LALWAC>2.0.CO;2.

- Bolton, D., 1980: The computation of equivalent potential temperature. *Mon. Wea. Rev.*, **108**, 1046–1053, doi:10.1175/1520-0493(1980)108<1046:TCOEPT>2.0.CO;2.
- Boutle, I. A., J. E. J. Eyre, and A. P. Lock, 2014: Seamless stratocumulus simulation across the turbulent gray zone. *Mon. Wea. Rev.*, **142**, 1655–1668, doi:10.1175/MWR-D-13-00229.1.
- Brinkmann, W. A. R., 1971: What is a foehn? *Weather*, **26**, 230–240, doi:10.1002/j.1477-8696.1971.tb04200.x.
- Cook, A. J., A. J. Fox, D. G. Vaughan, and J. G. Ferrigno, 2005: Retreating glacier fronts on the Antarctic Peninsula over the past half-century. *Science*, **308**, 541–544, doi:10.1126/science.1104235.
- Davies, T., M. J. P. Cullen, A. J. Malcolm, M. H. Mawson, A. Staniforth, A. A. White, and N. Wood, 2005: A new dynamical core for the Met Office's global and regional modelling of the atmosphere. *Quart. J. Roy. Meteor. Soc.*, **131**, 1759–1782, doi:10.1256/qj.04.101.
- Elvidge, A. D., I. A. Renfrew, J. C. King, A. Orr, and T. A. Lachlan-Cope, M. Weeks, and S. L. Gray, 2015: Foehn jets over the Larsen C Ice Shelf, Antarctica. *Quart. J. Roy. Meteor. Soc.*, **141**, 698–713, doi:10.1002/qj.2382.
- , —, —, —, —, 2016: Foehn warming distributions in nonlinear and linear flow regimes: A focus on the Antarctic Peninsula. *Quart. J. Roy. Meteor. Soc.*, doi:10.1002/qj.2489, in press.
- Fiedler, E. K., T. A. Lachlan-Cope, I. A. Renfrew, and J. C. King, 2010: Convective heat transfer over thin ice covered coastal polynyas. *J. Geophys. Res.*, **115**, C10051, doi:10.1029/2009JC005797.
- Gaffin, D. M., 2002: Unexpected warming induced by foehn winds in the lee of the Smoky Mountains. *Wea. Forecasting*, **17**, 907–915, doi:10.1175/1520-0434(2002)017<0907:UWIBFW>2.0.CO;2.
- , 2009: On high winds and foehn warming associated with mountain-wave events in the western foothills of the southern Appalachian mountains. *Wea. Forecasting*, **24**, 53–75, doi:10.1175/2008WAF2007096.1.
- Gedalof, Z., D. L. Peterson, and N. J. Mantua, 2005: Atmospheric, climatic, and ecological controls on extreme wildfire years in the northwestern United States. *Ecol. Appl.*, **15**, 154–174, doi:10.1890/03-5116.
- Hann, J., 1901: *Lehrbueh der Meteorologic*. 1st ed. Leipzig, 805 pp.
- Hoinka, K. P., 1985: What is a foehn clearance? *Bull. Amer. Meteor. Soc.*, **66**, 1123–1132, doi:10.1175/1520-0477(1985)066<1123:WIAFC>2.0.CO;2.
- Hunt, J. C. R., H. Olafsson, and P. Bougeault, 2001: Coriolis effects on orographic and mesoscale flows. *Quart. J. Roy. Meteor. Soc.*, **127**, 601–633, doi:10.1002/qj.49712757218.
- Kuipers Munneke, P., M. R. van den Broeke, J. C. King, T. Gray, and C. H. Reijmer, 2012: Near-surface climate and surface energy budget of Larsen C Ice Shelf, Antarctic Peninsula. *Cryosphere*, **6**, 353–363, doi:10.5194/tc-6-353-2012.
- Lock, A. P., A. R. Brown, M. R. Bush, G. M. Martin, and R. N. B. Smith, 2000: A new boundary layer mixing scheme. Part I: Scheme description and single-column model tests. *Mon. Wea. Rev.*, **128**, 3187–3199, doi:10.1175/1520-0493(2000)128<3187:ANBLMS>2.0.CO;2.
- Lothon, M., A. Druilhet, B. Bénéch, B. Campistron, S. Bernard, and F. Said, 2003: Experimental study of five föhn events during the Mesoscale Alpine Programme: From synoptic scale to turbulence. *Quart. J. Roy. Meteor. Soc.*, **129**, 2171–2193, doi:10.1256/qj.02.30.
- Mayr, G. J., and Coauthors, 2007: Gap flows: Results from the Mesoscale Alpine Programme. *Quart. J. Roy. Meteor. Soc.*, **133**, 881–896, doi:10.1002/qj.66.
- Meyers, M. P., and W. J. Steenburgh, 2013: Mountain weather prediction: Phenomenological challenges and forecast methodology. *Mountain Weather Research and Forecasting*, F. K. Chow, S. F. J. De Wekker, and B. J. Snyder, Eds., Springer, 1–34.
- Miltenberger, A. K., S. Pfahl, and H. Wernli, 2013: An online trajectory module (version 1.0) for the nonhydrostatic numerical weather prediction model COSMO. *Geosci. Model Dev.*, **6**, 1989–2004, doi:10.5194/gmd-6-1989-2013.
- Ólafsson, H., 2005: The heat source of the foehn. *Hrvat. Meteor. Časopis*, **40**, 542–545.
- Orr, A., T. Phillips, S. Webster, A. D. Elvidge, M. Weeks, J. S. Hosking, and J. Turner, 2014: Met Office Unified Model high-resolution simulations of a strong wind event in Antarctica. *Quart. J. Roy. Meteor. Soc.*, **140**, 2287–2297, doi:10.1002/qj.2296.
- Richner, H., and P. Hächler, 2013: Understanding and forecasting Alpine foehn. *Mountain Weather Research and Forecasting: Recent Progress and Current Challenges*, F. K. Chow, S. F. J. De Wekker, and B. J. Snyder, Eds., Springer, 219–260.
- Scorer, R. S., 1978: *Environmental Aerodynamics*. Vol. 815. Ellis Horwood, 488 pp.
- Seibert, P., 1990: South foehn studies since the ALPEX experiment. *Meteor. Atmos. Phys.*, **43**, 91–103, doi:10.1007/BF01028112.
- , H. Feldmann, B. Neininger, M. Bäuml, and T. Trickl, 2000: South foehn and ozone in the eastern Alps—Case study and climatological

- aspects. *Atmos. Environ.*, **34**, 1379–1394, doi:10.1016/S1352-2310(99)00439-2.
- Sharples, J. J., G. A. Mills, R. H. D. McRae, and R. O. Weber, 2010: Foehn-like winds and elevated fire danger conditions in southeastern Australia. *J. Appl. Meteor. Climatol.*, **49**, 1067–1095, doi:10.1175/2010JAMC2219.1.
- Smith, R. B., 1990: Why can't stably stratified air rise over high ground? *Atmospheric Processes over Complex Terrain, Meteor. Monogr.*, No. 45, Amer. Meteor. Soc., 105–107.
- Svensson, G., and Coauthors, 2011: Evaluation of the diurnal cycle in the atmospheric boundary layer over land as represented by a variety of single-column models: The second GABLS experiment. *Bound.-Layer Meteor.*, **140**, 177–206, doi:10.1007/s10546-011-9611-7.
- Vosper, S., E. Carter, H. Lean, A. Lock, P. Clark, and S. Webster, 2013: High resolution modelling of valley cold pools. *Atmos. Sci. Lett.*, **14**, 193–199, doi:10.1002/asl2.439.
- , J. K. Hughes, A. P. Lock, P. F. Sheridan, A. N. Ross, B. Jemmett-Smith, and A. R. Brown, 2014: Cold-pool formation in a narrow valley. *Quart. J. Roy. Meteor. Soc.*, **140**, 699–714, doi:10.1002/qj.2160.
- Wernli, B., and H. C. Davies, 1997: A Lagrangian-based analysis of extratropical cyclones. I: The method and some applications. *Quart. J. Roy. Meteor. Soc.*, **123**, 467–489, doi:10.1002/qj.49712353811.
- Westerling, A. L., D. R. Cayan, T. J. Brown, B. L. Hall, and L. G. Riddle, 2004: Climate, Santa Ana winds and autumn wildfires in southern California. *Eos, Trans. Amer. Geophys. Union*, **85**, 289–296, doi:10.1029/2004EO310001.
- Whiteman, C. D., and J. G. Whiteman, 1974: A historical climatology of damaging downslope windstorms at Boulder, Colorado. NOAA Tech. Rep. ERL 336-APCL 35, 62 pp.
- World Meteorological Organization, 1992: *International Meteorological Vocabulary*. Vol. 182. World Meteorological Organization, 784 pp.
- Zängl, G., B. Chimani, and C. Häberli, 2004: Numerical simulations of the föhn in the Rhine Valley on 24 October 1999 (MAP IOP 10). *Mon. Wea. Rev.*, **132**, 368–389, doi:10.1175/1520-0493(2004)132<0368: NSOTFI>2.0.CO;2.

## CLIMATE CHANGE/POLICY

*“This book is timely because global climate change policy is a mess.... Drawing on concrete examples and a broad range of social science theory, this book convincingly makes the case for a social learning approach to both adaptation and emissions mitigation.”*

— Steve Rayner, James Martin Professor of Science and Civilization, University of Oxford

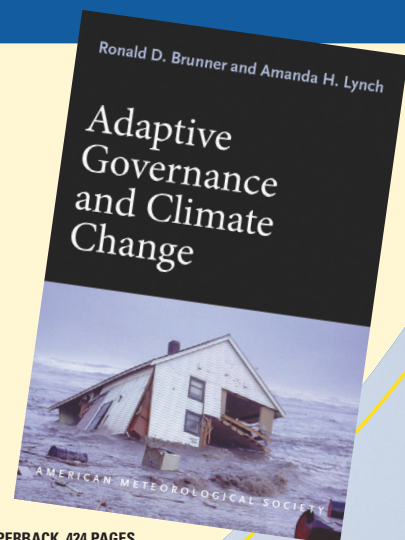
### Adaptive Governance and Climate Change

RONALD D. BRUNNER AND AMANDA H. LYNCH

As greenhouse gas emissions and temperatures at the poles continue to rise, so do damages from extreme weather events affecting countless lives. Meanwhile, ambitious international efforts to cut emissions have proved to be politically ineffective or infeasible. There is hope, however, in adaptive governance—an approach that has succeeded in some communities and can be undertaken by others around the globe.

In this book:

- A political and historical analysis of climate change policy
- How adaptive governance works on the ground
- Why local, bottom-up approaches should complement global-scale negotiations



© 2010, PAPERBACK, 424 PAGES

ISBN: 978-1-878220-97-4

AMS CODE: AGCC

LIST \$35 MEMBER \$22

## AMS BOOKS

RESEARCH APPLICATIONS HISTORY

[www.ametsoc.org/amsbookstore](http://www.ametsoc.org/amsbookstore)